Journal of Instrumentation

Fabrication and beam test of a silicon-tungsten electromagnetic calorimeter

To cite this article: S. Muhuri *et al* 2020 *JINST* **15** P03015

View the article online for updates and enhancements.

IOP ebooks™

Bringing together innovative digital publishing with leading authors from the global scientific community.

Start exploring the collection–download the first chapter of every title for free.

This content was downloaded from IP address 131.211.12.11 on 07/01/2021 at 14:16

Published by IOP Publishing for Sissa Medialab
Received: November 5, 2019
Revised: January 9, 2020
Accepted: February 11, 2020
Published: March 18, 2020

Fabrication and beam test of a silicon-tungsten electromagnetic calorimeter

S. Muhuri,[a,1] **S. Mukhopadhyay,**[b] **V.B. Chandratre,**[b] **T.K. Nayak,**[a,e] **S. Kumar Saha,**[a] **S. Thakur,**[a] **R.N. Singaraju,**[a] **J. Saini,**[a] **A. van den Brink,**[c] **T. Chujo,**[d] **R. Nath Patra,**[a] **M. van Leeuwen,**[c,e] **S. Ahmad Khan,**[a] **M. Sukhwani,**[b] **G.-J. Nooren**[c] **and T. Peitzmann**[c]

[a] *Experimental High Energy Physics and Application Group, Variable Energy Cyclotron Centre, HBNI, Kolkata — 700064, India*

[b] *Electronics Division, Bhabha Atomic Research Centre, HBNI, Trombay, Mumbai — 400085, India*

[c] *Institute for Subatomic Physics, Utrecht University and Nikhef, PO Box 80000, 3508TA Utrecht, The Netherlands*

[d] *University of Tsukuba, Tsukuba, Ibaraki 305-8577, Japan*

[e] *ALICE, CERN, Geneva 23, Switzerland*

E-mail: sanjibmuhuri@vecc.gov.in

Abstract: A silicon-tungsten (Si-W) sampling calorimeter, consisting of 19 alternate layers of silicon pad detectors (individual pad area of 1 cm^2) and tungsten absorbers (each of one radiation length), has been constructed for measurement of electromagnetic showers over a large energy range. The signal from each of the silicon pads is readout using an ASIC with a dynamic range from −300 fC to +500 fC. Another ASIC with a larger dynamic range, ±600 fC has been used as a test study. The calorimeter was exposed to pion and electron beams at the CERN Super Proton Synchrotron (SPS) to characterise the response to minimum ionising particles (MIP) and showers from electromagnetic (EM) interactions. Pion beams of 120 GeV provided baseline measurements towards the understanding of the MIP behaviour in the silicon pad layers, while electron beams of energy from 5 GeV to 60 GeV rendered detailed shower profiles within the calorimeter. The energy deposition in each layer, the longitudinal shower profile, and the total energy deposition have been measured for each incident electron energy. Linear behaviour of the total measured energy (E) with that of the incident particle energy (E_0) ensured satisfactory calorimetric performance. For a subset of the data sample, selected based on the cluster position of the electromagnetic shower of the incident electron, the dependence of the measured energy resolution on E_0 has been found to be $\sigma/E = (15.36/\sqrt{E_0(\mathrm{GeV})} \oplus 2.0)\%$.

Keywords: Calorimeter methods; Calorimeters

ArXiv ePrint: 1911.00743

[1] Corresponding author.

© 2020 CERN. Published by IOP Publishing Ltd on behalf of Sissa Medialab. Original content from this work may be used under the terms of the Creative Commons Attribution 3.0 licence. Any further distribution of this work must maintain attribution to the author(s) and the title of the work, journal citation and DOI.

https://doi.org/10.1088/1748-0221/15/03/P03015

2020 JINST 15 P03015

Contents

2020 JINST 15 P03015

1 Introduction

Electromagnetic sampling calorimeters, consisting of alternating layers of thin tungsten absorber and granular silicon sensors have been under active study for the last two decades for applications in high-energy physics experiments. In the present era of large-scale experiments at the Large Hadron Collider (LHC), Relativistic Heavy Ion Collider (RHIC), Japan Proton Accelerator Research Complex (J-PARC), Facility for Antiproton and Ion Research (FAIR) and proposed International Linear Collider (ILC), the field of calorimetry is constantly evolving, adapting to new technologies and new ideas. An example of a physics study using such a calorimeter is to constrain the low-x parton structure of protons and nuclei via the measurement of direct photons at the LHC. This requires, in particular, the discrimination of single photons from the dominating number of decay photons arising from neutral pions (π^0) and η. Measurement of the decay photons and reconstruction of the parent particles requires a calorimeter with fine granularity with excellent two-shower separation capability [1–4]. Thus one of the primary objectives of the present calorimeter is to provide position and energy measurements of photons and thereby γ-π^0 discrimination within a large momentum range ($\approx$ up to 50 GeV/c). Segmented sampling calorimeters with alternate passive and active media have the advantage to provide more differential measurements of particle showers [6–20] with an

energy resolution of the order of a few % at high energy. Segmentation in both longitudinal and transverse directions helps in particle identification, providing better γ-π^0 and γ-charged hadron discrimination compared to other available calorimetric options. A highly segmented calorimeter can also offer advantages for jet measurements when using particle flow algorithms [21].

Silicon sensors are most suitable as detection medium in high-energy physics experiments because of their good charge collection efficiency, fast response time and low bias voltage to achieve full depletion. Low sensitivity to magnetic fields makes silicon attractive for experiments with large ambient magnetic fields. As a converter material, tungsten is most suitable because of the small Moliere radius, which facilitates the containment of the energy of the incident particles fully in relatively small volumes. Sampling calorimeters using silicon and tungsten have been proposed for upgrades of the ALICE [29] and CMS [30] experiments at the LHC as well as in other contemporary experiments. Based on GEANT simulation studies [18] and a feasibility test with only a few layers [4], a 19 layer prototype Si-W calorimeter has been fabricated and tested with pion and electron beams at the CERN-SPS. The tungsten absorbers are of one radiation length (X_0) thickness, which results in a total depth of the calorimeter of about $19X_0$.

In this article, we present the design of the calorimeter along with readout electronics and discuss the test beam results. In section 2, we discuss the design and optimisation of the sampling calorimeter. In section 3, we present the calorimeter setup and electronics readout. The test beam setup at the SPS with trigger logic as well as the electronics noise for each detector pad are discussed in section 4. Results for pions incident on the calorimeter are presented in section 5. The response of the silicon layers to electron beams at different energies is presented in section 6 and compared to simulated results. In section 7, we present the results for energy resolution of the calorimeter. The article concludes with a summary in section 8.

2 Design and optimisation of the Si-W calorimeter

Geometry optimisation and characterisation of a sampling Si-W electromagnetic calorimeter have been carried out using the GEANT4 [23, 25] geometry package. The main goal is to optimise the geometry to achieve a good position and energy resolution in a high particle density environment. In total 19 layers, each consisting of silicon pad arrays and tungsten absorber have been implemented. The silicon pads are of 1 cm^2 area and 300 μm in thickness. A gap of 3mm was kept for electronics and readout behind each silicon pad layer. High purity tungsten plates of density 19.3gm/ cm^3 and dimension 10 cm×10 cm with 0.35 cm thickness have been placed alternately with silicon layers. The calorimeter setup is shown in figure 1.

In high-energy collisions, measurements of direct photons (which are not coming from hadronic decays) are of particular interest since they directly probe partonic processes. Direct photons originate directly from hard interactions, such as quark-anti-quark annihilation, quark-gluon Compton scattering, and higher order processes. In experiments, the large background of photons from hadronic decays is partially removed by selections and the remaining background is subtracted to determine the direct photon cross section. One of the selection cuts that is frequently employed is a so-called isolation cut that selects photons that are not accompanied by additional momentum flow; such a cut rejects both decay photons from quark and gluon jets as well as so-called fragmentation photons, which are produced as radiation off a high-energy quark. The rejection and subtraction

2020 JINST 15 P03015

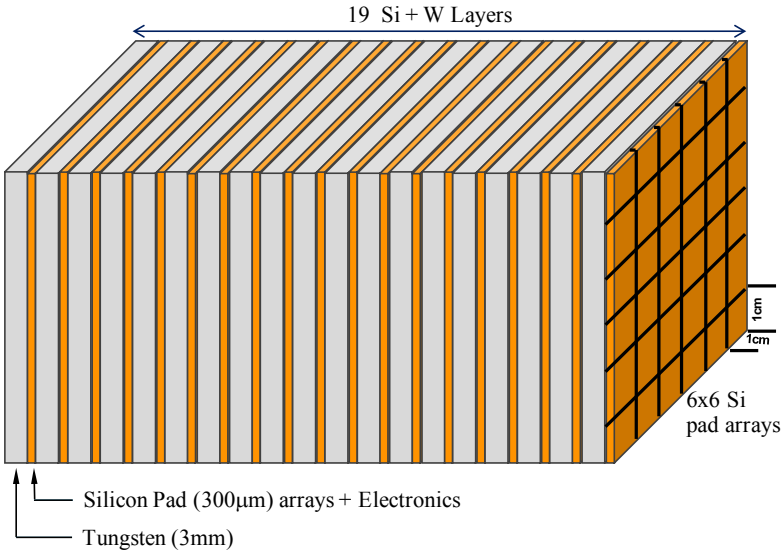

Figure 1. The components of a silicon-tungsten sampling calorimeter consisting of 19 alternating layers of silicon pad detectors (individual pad area of 1 cm^2) and tungsten plates (1 X_0 thick).

of the contributions from hadronic decays requires an accurate reconstruction of π^0 and η from its decay photons. The energy deposition is measured in each individual pad sensor of each silicon layer. The photon showers are reconstructed in the silicon layers, which provide the position of the shower center, shower shape, and total energy deposition.

With the increase of the parent π^0 energy, the opening angle between the decay photons decreases, which is not possible to measure with the above configuration of the calorimeter. To improve the measurement of two-shower separations, a modified setup has been planned in the future by including two or three very high granularity silicon pixel (of size 1 mm^2) layers at depths around the shower maximum. Studies with a high-granularity calorimeter using pixel sensors are reported elsewhere [22].

3 Calorimeter setup

Figure 2 shows a photograph of the calorimeter setup. A custom-designed mechanical arrangement for holding the tungsten plates and silicon pad detectors properly in place has been constructed. The average gap between two consecutive tungsten layers was kept at 0.4 cm to accommodate a silicon detector mounted on a 0.08 cm thick PCB and the associated electronics.

3.1 Silicon pad array

6×6 arrays of silicon pad detectors with 1 cm^2 individual pad size are developed on 4-inch wafers with 36 pads per detector layer. The detectors were fabricated [5] on 300μm-thin n-type FZ (Float-Zone) wafers with $\langle 111 \rangle$ crystal orientation. Figure 3 shows a photograph of such a silicon detector layer. The starting resistivity of the wafer is 4-5 kΩ-cm. The p-n junctions are created by implanting p-type impurity from the top side. High breakdown voltage and low leakage current are

2020 JINST 15 P03015

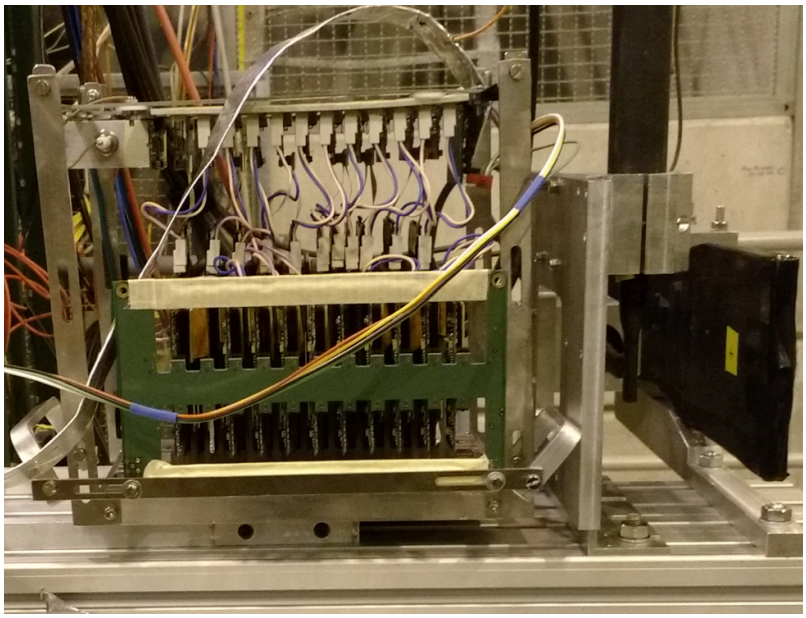

Figure 2. Experimental arrangement of the Si-W prototype calorimeter with 19 layers of silicon pad detectors arrays and tungsten plates along with associated electronics for the beam test at CERN-SPS.

the essential features of silicon pad detectors for HEP experiments to compensate the performance degradation due to long term operation under large particle fluence. The design of the silicon pad is carried out with multiple FGR (Floating Guard Rings) and MO (Metal Overhang) over the individual pad to reduce the electric field crowding at the junction edge near the surface and thus improving the breakdown voltage [35]. Moreover gettering techniques and double implantation steps for the backside ohmic contact have been incorporated to reduce the leakage current of the large area silicon detectors. Alignment sites are placed in each pad for checking the integrity of an individual pad connection. The silicon pad detectors are designed with a conventional wire bonding packaging option. Due to limitations of the foundry, all the interconnections have to make use of a single metal layer. The distances and routing have been optimized to ensure minimum cross-talk among the pads and a minimal dead area.

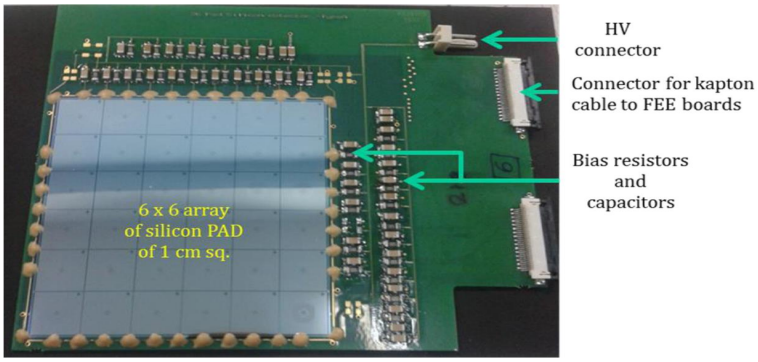

Figure 3. Silicon detector array consisting of 6×6 pads (each of 1 cm^2 area).

2020 JINST 15 P03015

The silicon pads are die-attached and mounted on a 0.8 mm-thick four-layer PCB with a silver conductive epoxy of resistivity 0.006 Ω-cm followed by gold wire bonding from each pad to the PCB. The fabricated and packaged detectors have less than 10nA/ cm^2 leakage current with a breakdown voltage of more than 500 V. With full depletion achieved around 45 V, each pad has 45–50 pF/ cm^2 detector capacitance.

3.2 Readout electronics

The detector signals were readout using front-end electronics boards making use of two different readout ASICs, called MANAS and ANUSANSKAR. Both ASICs have 16 low-noise pulse processing channels. Each channel is comprised of Charge Sensitive Amplifier, semi Gaussian shaper, track and hold and analog serial data readout. The linear dynamic range of MANAS is from +500 fC to −300 fC, while ANUSANSKAR ASIC has a dynamic range of ±600 fC. The results presented in this report are based on data taken with MANAS as readout ASIC.

In each pad layer, 32 pads out of 36 are connected to the readout electronics, excluding the four corner pads. This is because the readout board contains 64 channels and so for ease of connection two pad layers are connected to one readout board. In total 19×32 electronics channels are connected to the pad detectors. The beam was incident at the center of one of the central pads. As the transverse shower spread is expected to be about 1 cm, the exclusion of the corner pads is not expected to significantly affect the measurement of the shower properties.

4 Test beam setup at CERN-SPS

The Si-W calorimeter has been tested using the H6 beamline facility [33] of the CERN SPS. In this beamline, secondary particle beams provide hadrons, electrons or muons at momenta between 5 GeV/c and 205 GeV/c, depending on the setup. Three distinct modes of operation are possible in this beamline, which are the high-resolution mode, the high transmission mode and the filter mode or test-beam mode. Here, the filter mode has been used for the beam operation, which gives a large range of incident energies. Maximum intensities achievable with the H6 beamline for 10^{12} primary protons at 400 GeV/c are 10^8 and 4×10^7 for π^+ and π^-, respectively at 150 GeV/c. For optimising the purity of the electron beam, a Cherenkov detector is used as a part of the beamline setup.

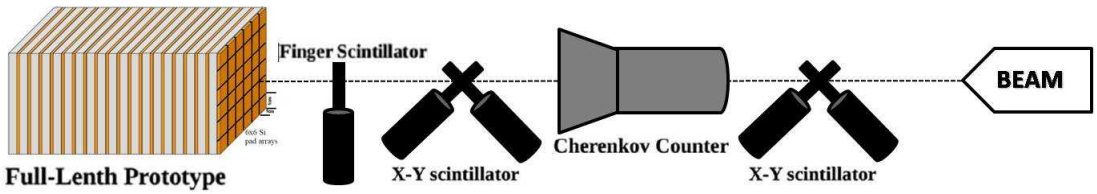

Figure 4. Schematic setup of the Si-W calorimeter along with the trigger arrangement for beam tests at CERN-SPS.

The calorimeter was placed in the H6 beam hall on an adjustable table, capable of moving both in horizontal and vertical directions. The movements could be controlled remotely from the counting room. All the detector layers were properly shielded against both electromagnetic

2020 JINST 15 P03015

interference and ambient light to improve the signal to noise ratio. The readout ASICs placed close to silicon detectors, were coupled to the CROCUS data acquisition via the MARC ASIC interface [27, 28]. The data were sent to the counting room through optical fiber cables.

A dedicated trigger setup, with two pairs of scintillator paddles and a finger scintillator, was used to define the beam. The trigger arrangement is shown in figure 4. The two pairs of scintillator paddles define the $X - Y$ position of the incoming beam within 1 cm^2 area whereas the small finger scintillator (3mm×3mm) helps to position the beam mostly within a single silicon pad. The coincidence signal from the scintillator paddles and the finger scintillator was used to select the beam. Electrons were filtered using the Cherenkov detector in addition to the scintillators.

The electronics noise arising both from the detector and the readout has been measured for each channel of the calorimeter without the beam, which gives the pedestal of the ADC distribution. For a given channel, the pedestal is defined by the mean value of the ADC and the corresponding RMS deviation. In figure 5, we plot the mean and RMS of the pedestal for each silicon pad (each electronics channel). The mean values were consistently in the vicinity of 250 ADC counts and were stable with time. The RMS (representing the noise) were between 1.5 to 2.5 ADC counts. Some fluctuations have been observed in the RMS distributions in some of the channels, where RMS values are either very large (noisy channels) or have values close to zero (dead channels). This can arise because of processing errors at the foundry level or because of faulty electronics. During the next iteration of the detector, care will be taken to minimize these faults. There were 65 such noisy/dead cells out of the 608 total. For calculating the total response from the EM showers, these channels are assigned ADC values which are averages of their adjacent channels.

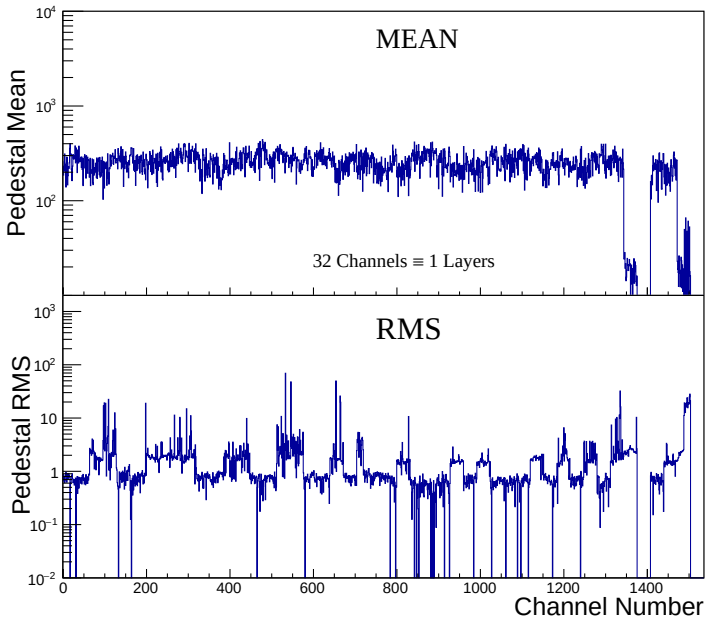

Figure 5. Pedestal mean (upper panel) and RMS (lower panel) as a function of detector channel number. Groups of 32 channels correspond to individual layers along the depth of the calorimeter.

2020 JINST 15 P03015

In the present analysis, each pad response is obtained by subtracting the pedestal (mean) from the measured ADC counts. The pad response corresponds to the amount of deposited energy in the silicon pad. A sum of the pad response over the entire layer gives the response of the silicon pad layer.

5 Response of the calorimeter to pion beam

The Si-W calorimeter has been exposed to pion beams at an incident energy of 120GeV. Because the finger scintillator is placed at the center of one of the silicon pads, most of the time only this center pad is hit. The distribution of the single layer response as measured by the second silicon detector layer is shown in the upper panel of figure 6. The data points are plotted after pedestal subtraction. Minimum ionising particles are selected by applying a condition on the total energy deposited in an event within the whole calorimeter prototype. The data in figure 6 is plotted for a particular pad in a layer. The histogram is fitted with a Landau distribution, which gives a most probable value (MPV) of 18.0±2.5. This is similar to what was obtained in an earlier test beam [4] without any material in front of the silicon detector. A deviation can be found between 50 to 100 in upper panel of figure 6 which might result a smaller peak at higher energy due to multiple hits. The corresponding (MPV) value of deposited energy from the simulation is 0.083 MeV as shown in the lower panel of figure 6.

6 Response of the calorimeter to electrons

Electrons incident on the Si-W calorimeter produce electromagnetic showers which leave hits distributed among pads in each of the layers. The response in each layer has been studied to understand the shower profile along the longitudinal direction. In general, showers induced by incident electrons produce signals in several pads; the number of pads depends on the incident energy.

6.1 Energy deposition in different layers

The distributions of the layer response for the 7^{th} layer are presented in figure 7 for incident electrons of six different energies, E_0 = 5, 20, 30, 40, 50 and 60 GeV. The ordinate is expressed in terms of probability, where the counts are normalised to the number of events. These measured response spectra have approximate Gaussian shapes, so mean values are extracted using Gaussian fits. The results of these fits are analysed below to obtain the longitudinal shower profile. Similar fits are performed to the sum of the signals to obtain the total response and the energy resolution of the prototype calorimeter.

6.2 Longitudinal shower profile

The longitudinal profile of the EM shower is obtained by plotting the measured mean of the response for each layer along the depth of the calorimeter, i.e. as a function of the layer number. Figure 8 shows the longitudinal shower profiles for different incident electron energies. Here each layer corresponds to $1.013X_0$. For all incident energies, the response increases as a function of layer number until it reaches a maximum value and then decreases gradually. The shower profile can be described by the empirical formula [31],

$$\frac{dR}{dt} = R_0 \cdot t^a \cdot e^{-bt}, \tag{6.1}$$

2020 JINST 15 P03015

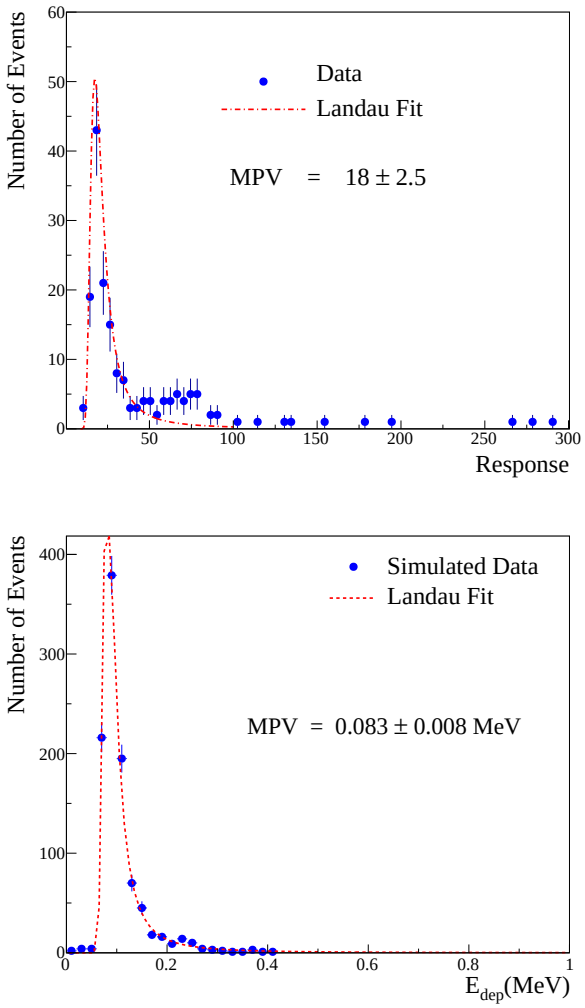

Figure 6. The top panel shows the measured response of silicon pad detectors to 120 GeV pions. The statistical uncertainties are small and within the marker size. The bottom panel gives the energy deposition in MeV from the simulated data. Both the distributions are fitted with a Landau function.

where R_0 is a normalisation parameter, $t = z/X_0$ is the thickness of the absorber in front of the layer in units of radiation length, and a and b are fit parameters describing the shape. The longitudinal shower profile has been fitted using this formula and the fitted curves are superimposed on the measured data points. These curves describe the data well. At higher energies, flatter regions are seen around the shower maximum position, which may be caused by saturation of the ADC of the MANAS readout.

The position of the shower maximum depends on the incident electron energy and can be expressed in terms of the fit parameters, a and b, as $t_{\max} = b/a$. The extracted values of the shower maximum have been plotted as a function of the incident energy in figure 9. The depth of the shower maximum position increases with the increase of the incident energy. The shower maximum position can also be described by the empirical formula [31]:

$$t_{\max} = \ln\left(\frac{E_0}{E_C}\right) + C_{e,\gamma}, \tag{6.2}$$

2020 JINST 15 P03015

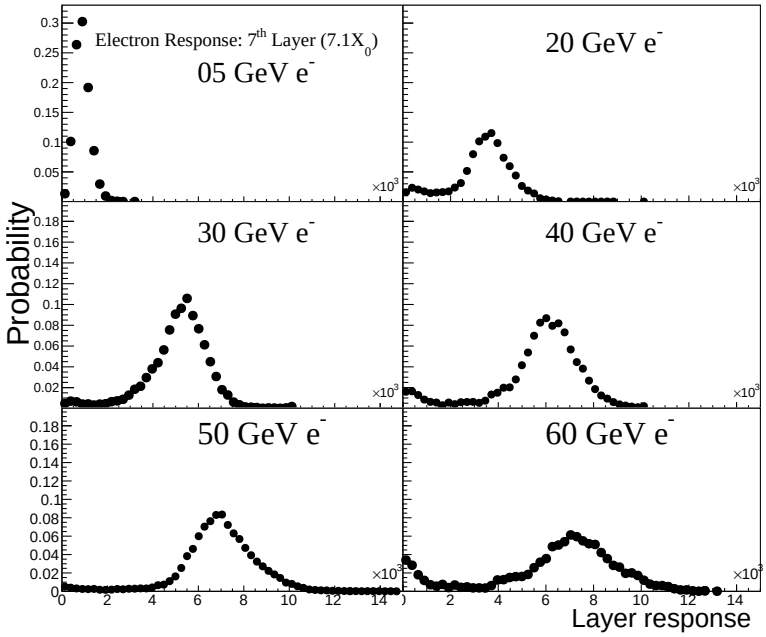

Figure 7. Measured response on the 7^{th} layer of the Si-W calorimeter for 5, 20, 30, 40, 50 and 60 GeV electrons. The statistical uncertainties are small, and within the size of the markers. Gaussian fits to the curves give the mean response.

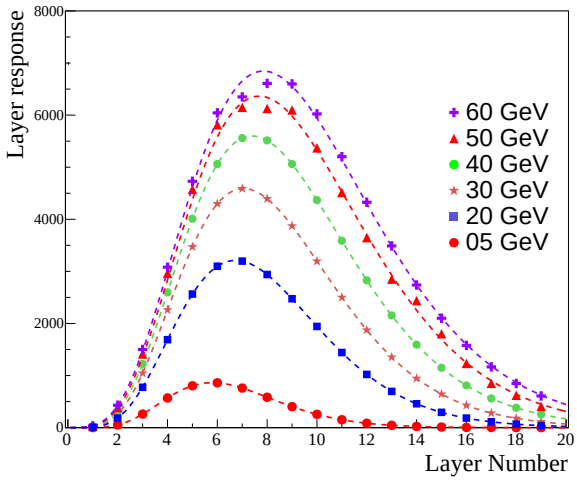

Figure 8. Longitudinal shower profiles of the Si-W calorimeter for 5, 20, 30, 40, 50 and 60 GeV electrons as a function of the silicon layer along the depth of the calorimeter. The statistical uncertainties are small and within the size of the markers. The data are fitted with an empirical curve as given in equation (6.1).

where E_C is the critical energy, at which the electron ionisation losses and bremsstrahlung losses become equal, given by $E_C = 550\text{MeV}/Z_{\text{eff}}$. $C_{e,\gamma}$ is a parameter, which takes different values for electrons and photons, here we use $C_e = -1.0$. The empirical formula is shown as the dashed curve in figure 9 and is seen to describe the data reasonably well.

2020 JINST 15 P03015

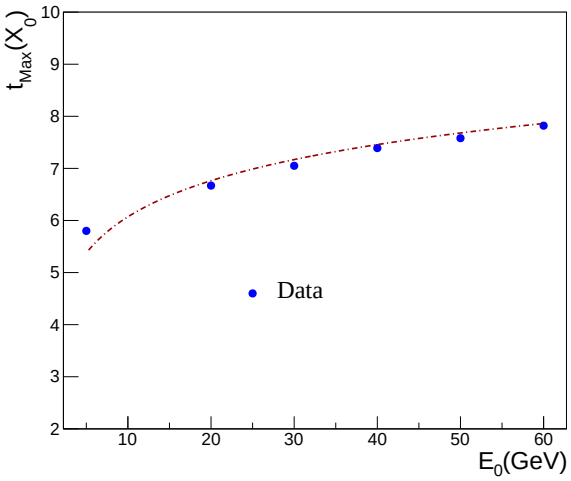

Figure 9. Position of the shower maximum in the Si-W calorimeter as a function of incident electron energy. The statistical errors are small and within the size of the markers. The line corresponds to the function given in equation (6.2).

7 Total energy response of the calorimeter

The total energy deposition in the calorimeter can be obtained by summing the pedestal-subtracted energy response (ADC) of the individual pads of the silicon layers. The details of the electromagnetic shower propagation inside the calorimeter can be better understood in terms of the parameters associated with the calorimetric responses to the energy deposition such as calibration, and energy resolution. However, it is to be noted that non-uniformity in the detector and the gaps in between the silicon wafer and tungsten do influence the response when showers traverse these regions [11]. In the absence of a direct estimation of such effects, we have studied the cluster position of the electromagnetic shower by projecting all the pad level signals onto a single layer of the calorimeter and selecting events which satisfy a criterion set on the position of the cluster centres on an event-by-event basis. The cluster centres (X_C, Y_C) are determined by calculating the centre of gravity with logarithmic weights, to improve the position resolution. The signals are first summed over all layers for each transeverse pad position and the centre of gravity is then calculated by summing over the pads:

$$X_C = \frac{\sum_i w_i x_i}{\sum_i w_i}, \tag{7.1}$$

where i is the pad index, x_i is the transverse position (in x) and $w_i = \max\left(0, \left[w_0 + \ln\left(\frac{E_i}{E_T}\right)\right]\right)$ is the weight, which depends on the energy deposition E_i in the pad and the total shower energy E_T. The y-coordinate of the centroid Y_C is calculated in the same way, using y_i instead of x_i. Events are selected to have their shower position in the active area that is selected by the trigger scintillator within a region of uniform response; the range $1.8 < X_C < 2.2$ cm and $2.5 < Y_C < 2.8$ cm is selected. The origin of the coordinate system is the lower left corner pad of the layer. It was verified that this selection does not bias the energy response significantly.

2020 JINST 15 P03015

7.1 Response to different incident energies

Figure 10 shows distributions of the total energy deposition in the calorimeter for six incident energies. Gaussian shapes have been observed for each incident energy and the distributions are well separated from each other. By fitting the distributions with Gaussian functions, we obtain the mean and width for each energy which are used to charaterize the detector response.

Figure 11 shows the mean of the total response as a function of the incident energy of electrons. A linear response is found, except for the highest two energyes (50 and 60 GeV), where a saturation effect due to the limited dynamic range of the readout electronics has been indentified during the data analysis. A linear fit to the data points below 50 GeV yields: Response = $(1.390 \pm 0.038) \cdot 10^3 E_0/\mathrm{GeV}$, where E_0 is the incident beam energy.

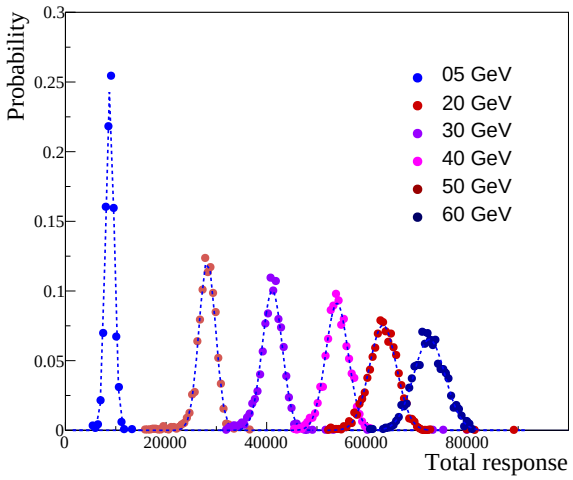

Figure 10. Response of the calorimeter for electrons, calculated using the selected events depending on the cluster centre position. The error bars represent statistical uncertainties.

7.2 Energy resolution

The energy resolution is one of the most important parameters to characterise a calorimeter. For a given incident energy, the resolution is defined as the ratio of the width (σ) to the mean (E) of the measured energy or the total energy response. Figure 12 shows the measured energy resolution (σ/E) of the calorimeter, plotted as a function of the incident energy. With the increase of the incident energy, resolution decreases. The measured energy resolution includes the combined effects of the structure of the calorimeter, the statistical fluctuations of the shower development, and contribution from electronic noise. The energy dependence of the resolution of a calorimeter is normally expressed in terms of the following empirical formula [14, 34]:

$$\frac{\sigma}{E} = a \oplus \frac{b}{\sqrt{E_0/\mathrm{GeV}}}, \tag{7.2}$$

where a and b are the fit parameters. The coefficient b gives the contribution from fluctuations in the shower development, which have a characteristic $\frac{1}{\sqrt{E}}$ dependence, while a quantifies the

2020 JINST 15 P03015

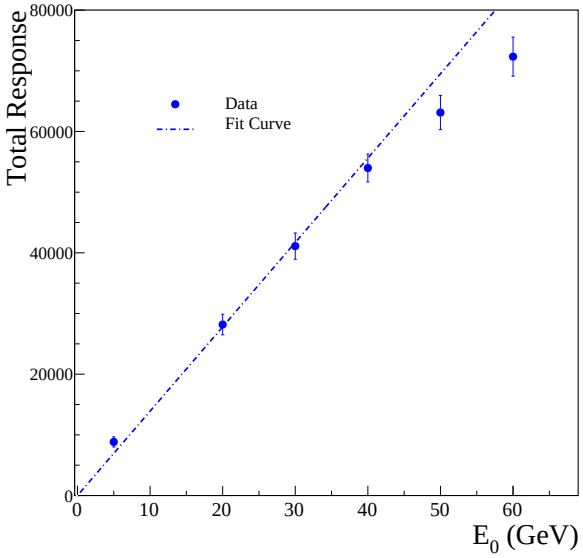

Figure 11. Total measured energy deposition for events. The error bars represent statistical uncertainties. A linear fit of the form $f = (1.390 \pm 0.038) \cdot 10^3 E_0/\text{GeV}$ can explain the data well.

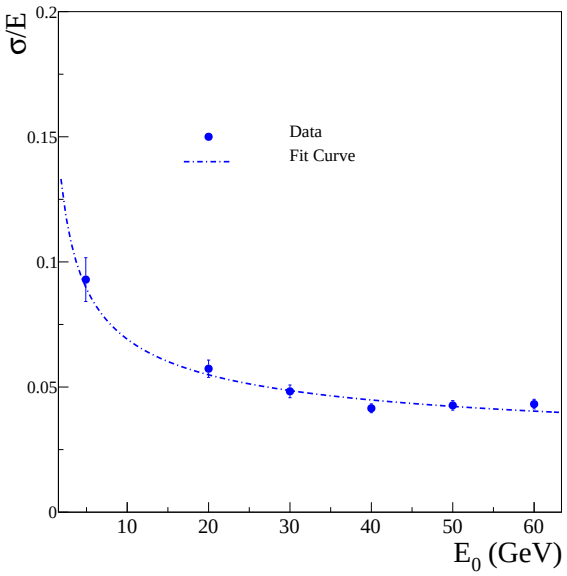

Figure 12. Measured energy resolution of the Si-W calorimeter prototype. The error bars represent statistical uncertainties. A fit for the form, $\frac{\sigma}{E} = a \oplus \frac{b}{\sqrt{E_0/\text{GeV}}}$, with $a = 0.020 \pm 0.0038$ and $b = 0.1536 \pm 0.023$, fits the data points very well.

energy-independent contribution. The constant term specifies the imperfections in the construction of the calorimeter and is sensitive to non-uniform response of the detector. It is crucial to have a low value of the constant term (about 1%) to achieve good energy resolution at high energy. A fit

2020 JINST 15 P03015

of this form to the calorimetric data of figure 12 yields, $a = 0.02 \pm 0.003$ and $b = 0.1536 \pm 0.023$. These coefficients, expressed in terms of percentage are: $\sigma/E = 15.36/\sqrt{E_0(\mathrm{GeV})} \oplus 2.0$ (%). This effect has been studied using GEANT4 simulation with an approximate detector geometry. The measured resolution is close to what has been estimated from the simulation. It is worth mentioning here that the constant term a of 2% can be improved by making the calorimeter more compact, by the use of improved readout electronics and with proper relative calibration of the individual pads.

8 Summary

A prototype Si-W calorimeter has been designed, constructed and tested using pion and electron beams at different energies at the CERN SPS. The calorimeter comprises of 19 layers of silicon pad and tungsten layers placed alternating with each other. The silicon pads are of 1 cm^2 area and 300 μm thick, and the tungsten plates are of $1X_0$ thick. For the readout the MANAS ASIC has been used, which has a limited dynamic range. The calorimeter was tested with 120GeV pion beams to understand the behaviour of minimum ionising particles. Electron beams of energy 5 to 60 GeV provided the electromagnetic showers for each silicon layer of the detector. Longitudinal shower profiles have been obtained from which the position of the shower maximum has been extracted. The total response for different incident energy electrons has been obtained. A linear behaviour of measured total energy with that of incident energy ensures satisfactory calorimetric performance. The dependence of the measured energy resolution on the incident beam energy E_0 can be characterised as $\sigma/E = 15.3/\sqrt{E_0(\mathrm{GeV})} \oplus 2$ (%). These results are comparable to the ones obtained by the CALICE collaboration [11] for an equivalent silicon-tungsten sampling calorimeter.

Acknowledgments

We acknowledge valuable discussions held with Yogendra P. Viyogi, Sinjini Chandra, Premomoy Ghosh, and Subhasish Chattopadhyay. We thank Bharat Electronics Limited, Bangalore for providing the silicon pad detectors. We thank the CERN SPS crew for providing excellent quality beam for the detector tests and ALICE-FOCAL collaboration for the support during the tests.

References

[1] ALICE FoCal collaboration, *Measurement of forward direct photon production in p-A at the LHC with ALICE — a probe for nuclear PDFs and saturation*, PoS(DIS2016)273 (2016) [arXiv:1607.01673].

[2] M. Krelina, J. Cepila and J. Nemchik, *Challenges of direct photon production at forward rapidities and large p_T*, *J. Phys. Conf. Ser.* **805** (2017) 012003.

[3] C.W. Fabjan and F. Gianotti, *Calorimetry for particle physics*, *Rev. Mod. Phys.* **75** (2003) 1243.

[4] S. Muhuri et al., *Test and characterization of a prototype silicon-tungsten electromagnetic calorimeter*, *Nucl. Instrum. Meth.* **A 764** (2014) 24 [arXiv:1407.5724].

[5] *Bharat Electronics Ltd., Central Research Laboratory webpage*, http://www.bel-india.in/, Bangalore, India.

2020 JINST 15 P03015

[6] G. Barbiellini et al., *Energy resolution and longitudinal shower development in a Si/W electromagnetic calorimeter*, *Nucl. Instrum. Meth.* **A 235** (1985) 55.

[7] G. Barbiellini et al., *Electromagnetic shower development in uranium and tungsten: a comparison of data from a silicon sampling calorimeter*, *Nucl. Instrum. Meth.* **A 236** (1985) 316.

[8] G. Ferri et al., *The structure of lateral electromagnetic shower development in Si/W and Si/U calorimeters*, *Nucl. Instrum. Meth.* **A 273** (1988) 123.

[9] WIZARD collaboration, *The WIZARD/CAPRICE silicon-tungsten calorimeter*, *Nucl. Instrum. Meth.* **A 370** (1996) 403.

[10] OPAL collaboration, *Precision luminosity for Z^0 line shape measurements with a silicon tungsten calorimeter*, *Eur. Phys. J.* **C 14** (2000) 373 [hep-ex/9910066].

[11] CALICE collaboration, *Response of the CALICE Si-W electromagnetic calorimeter physics prototype to electrons*, *Nucl. Instrum. Meth.* **A 608** (2009) 372 [arXiv:0811.2354].

[12] CALICE collaboration, *Semiconductor sensors for the CALICE SiW EMC and study of the cross-talk between guard rings and pixels in the CALICE SiW prototype*, *J. Phys. Conf. Ser.* **160** (2009) 012067.

[13] G. Mavromanolakis, *CALICE silicon-tungsten electromagnetic calorimeter*, *Pramana J. Phys.* **69** (2007) 1063.

[14] CALICE collaboration, *Construction and testing of a large scale prototype of a silicon tungsten electromagnetic calorimeter for a future lepton collider*, *Nucl. Instrum. Meth.* **A 732** (2013) 470.

[15] E. Kistenev, *Silicon-tungsten calorimeter for the forward direction in the PHENIX experiment at RHIC*, *Czech. J. Phys.* **55** (2005) 1659.

[16] V. Bonvicini et al., *Silicon-tungsten calorimeter for the forward direction in the PHENIX experiment at RHIC*, *IEEE Trans. Nucl. Sci.* **52** (2005) 874.

[17] D.M. Strom et al., *Fine grained silicon-tungsten calorimetry for a linear collider detector*, *IEEE Trans. Nucl. Sci.* **52** (2005) 868.

[18] R.P. Sandhir, S. Muhuri and T. Nayak, *Dynamic Fuzzy c-Means (dFCM) clustering and its application to calorimetric data reconstruction in high energy physics*, *Nucl. Instrum. Meth.* **A 681** (2012) 34 [arXiv:1204.3459].

[19] ALICE collaboration, *Prototype studies for a forward EM calorimeter in ALICE*, in *Proceedings, International Conference on Calorimetry for the High Energy Frontier (CHEF* 2013*)*, Paris, France, 22–25 April 2013, pg. 341 [arXiv:1308.2585].

[20] ALICE collaboration, *Small-x physics with the ALICE experiment at the CERN-LHC*, *Nucl. Phys.* **A 854** (2011) 230 [arXiv:1009.2220].

[21] J.C. Brient, *Improving the jet reconstruction with the particle flow method: an introduction*, in 11^{th} *international conference on calorimetry in high-energy*, Perugia, Italy 28 March–2 April 2004, World Scientific, Singapore (2005), pg. 445.

[22] A.P. de Haas et al., *The FoCal prototype — an extremely fine-grained electromagnetic calorimeter using CMOS pixel sensors*, 2018 *JINST* **13** P01014 [arXiv:1708.05164].

[23] GEANT4 collaboration, *GEANT4: a simulation toolkit*, *Nucl. Instrum. Meth.* **A 506** (2003) 250.

[24] T.C. Awes, F.E. Obenshain, F. Plasil, S. Saini, S.P. Sorensen and G.R. Young, *A simple method of shower localization and identification in laterally segmented calorimeters*, *Nucl. Instrum. Meth.* **A 311** (1992) 130.

2020 JINST 15 P03015

[25] J. Allison et al., *GEANT4 developments and applications*, *IEEE Trans. Nucl. Sci.* **53** (2006) 270.

[26] ALICE collaboration, *The muon spectrometer of the ALICE experiment*, *Nucl. Phys.* **A 749** (2005) 313 [hep-ex/0410061].

[27] P. Courtat et al., *The electronics of the ALICE dimuon tracking chambers*, ALICE Internal Note, ALICE-INT-2004-026, CERN, Geneva, Switzerland (2004).

[28] ALICE collaboration, *ALICE Photon Multiplicity Detector (PMD): addendum to the technical design report*, CERN-LHCC-2003-038, CERN, Geneva, Switzerland (2003) [ALICE-TDR-6].

[29] ALICE collaboration, *A Forward Calorimeter (FoCal) in the ALICE experiment*, ALICE-PUBLIC-2019-005, CERN, Geneva, Switzerland (2019).

[30] CMS collaboration, *HGCAL: a High-Granularity Calorimeter for the endcaps of CMS at HL-LHC*, *J. Phys. Conf. Ser.* **928** (2017) 012025.

[31] E. Longo and I. Sestili, *Monte Carlo calculation of photon initiated electromagnetic showers in lead glass*, *Nucl. Instrum. Meth.* **128** (1975) 283 [*Erratum ibid.* **135** (1976) 587].

[32] W.W.M. Allison and J.H. Cobb, *Relativistic charged particle identification by energy loss*, *Ann. Rev. Nucl. Part. Sci.* **30** (1980) 253.

[33] *Short introduction to the use of the H6 beam*, http://sba.web.cern.ch/sba/BeamsAndAreas/h6/H6manual.pdf.

[34] C.W. Fabjan and F. Gianotti, *Calorimetry for particle physics*, *Rev. Mod. Phys.* **75** (2003) 1243 [CERN-EP-2003-075].

[35] V. Mishra et al., *Studies on reducing leakage current and improving breakdown voltage of large-area silicon detectors: technology and results*, *Nucl. Instrum. Meth.* **A 527** (2004) 308.

2020 JINST 15 P03015